European Journal of Medicinal Chemistry 44 (2009) 4496–4508

Contents lists available at ScienceDirect

European Journal of Medicinal Chemistry

journal homepage: http://www.elsevier.com/locate/ejmech

Original article

Mapping the ribonucleolytic active site of bovine seminal ribonuclease. The binding of pyrimidinyl phosphonucleotide inhibitors

Kyriaki Dossi [a], Vicky G. Tsirkone [a], Joseph M. Hayes [a], Josef Matoušek [b,*], Pavla Poučková [c,*], Josef Souček [d], Marie Zadinova [c], Spyros E. Zographos [a], Demetres D. Leonidas [a,*]

[a] Institute of Organic and Pharmaceutical Chemistry, National Hellenic Research Foundation, 48 Vas. Constantinou Avenue, 11635 Athens, Greece
[b] Institute of Animal Physiology and Genetics, Academy of Sciences of The Czech Republic, Libechov 27721, Czech Republic
[c] Charles University in Prague, 1st Faculty of Medicine Kateřinská 32, Prague 2, 12000 Czech Republic
[d] Institute of Hematology and Blood Transfusion, Prague 2, Czech Republic

ARTICLE INFO

Article history:
Received 15 April 2009
Received in revised form
12 June 2009
Accepted 15 June 2009
Available online 29 July 2009

Keywords:
Bovine seminal ribonuclease
Enzyme inhibition
Drug design QikProp
ADME properties

ABSTRACT

Bovine seminal ribonuclease (BS-RNase) is a 27 kDa homodimeric enzyme and a member of the pancreatic RNase A superfamily. It is the only RNase with a quaternary structure and it is a mixture of two dimeric forms. In the most abundant form the active site is formed by the swapping of the N-terminal segments. BS-RNase is a potent antitumor agent with severe side effects such as aspermatogenicity, and immunosuppression. As a first step towards the design of potent inhibitors of this enzyme we mapped its active site through the study of the binding of uridine 2′-phosphate (U2′p), uridine 3′-phosphate (U3′p), uridine 5′-diphosphate (UDP), cytidine 3′-phosphate (C3′p), and cytidine 5-phosphate (C5′p), by kinetics, and X-ray crystallography. These phosphonucleotides are potent inhibitors with C3′p being the most potent with a K_i value of 22 μM. Absorption, distribution, metabolism, and excretion pharmacokinetic property predictions reveal U2′p, U3′p, and C5′p as the most promising with respect to oral bioavailability. In vivo studies on the aspermatogenic effect have shown that C3′p and C5′p inhibit significantly this biological action of BS-RNase.

1. Introduction

Bovine seminal ribonuclease (BS-RNase), a 27 kDa homodimeric ribonuclease with 83% sequence identity to bovine pancreatic Ribonuclease A (RNase A) is a potent antitumor agent [1]. The antitumor action of BS-RNase has been attributed to its ability to permeate only malignant cells and to reach the cytosol [2], where it degrades ribosomal RNA and blocks protein synthesis, causing cell death. BS-RNase is a promising antitumor agent and experiments have shown that administration of BS-RNase to animals with tumors has led to severe inhibition of neoplastic growth [3–6]. It has also been shown that BS-RNase selectively kills human multi-drug-resistant neuroblastoma cells via induction of apoptosis [7].

BS-RNase, like all RNase A homologs, catalyzes the cleavage of RNA at pyrimidine sites, by a transphosphorylation mechanism. However, BS-RNase is the only member of the RNase A superfamily with a quaternary structure and a potential allosteric site [8]. Native BS-RNase is a homodimer with two subunits (denoted as SA and SB) linked by a disulfide bridge between cysteines 31 and 32. The dimer of BS-RNase is a mixture of two quaternary forms, which differ in the position of the N-terminal α-helix. In the first form (denoted MxM) the N-terminal α-helix (residues 1–15) is swapped between the two subunits generating two composite active sites consisting of residues that belong to different subunits. In the second form, (denoted M = M) there is no exchange of the helices and each monomer conforms an independent entity. The two forms exist in a dynamic equilibrium in the solution with a ratio of MxM/M = M of 2. The conversion of one form to the other entails the exchange of N-terminal helices between subunits and it has been shown that the MxM form is responsible for cytotoxicity [9,10]. Despite these unusual properties, the amino acid sequences of BS-RNase and RNase A differ only in 23 residues and their active sites share a high degree of sequence and structural similarity. Their differences include 4 residues of the hinge peptide (residues 16–22) that connects the N-terminal fragment to the main body of the protein.

Abbreviations: BS-RNase, bovine seminal ribonuclease; RNase A, bovine pancreatic Ribonuclease A; 2′-deoxycytidine-2′-deoxyadenosine-3′,5′-monophosphate, 3′,5′-CpA; uridylyl-2′,5′-adenosine, 2′,5-UpA; uridylyl-2′,5′-phosphoguanosine, 2′,5′-UpG; PEG, poly(ethylene glycol); rms, root-mean-square; MES, 2-(N-morpholino)ethanesulfonic acid; ADME, Absorption Distribution Metabolism Excretion; cRI, cytoplasmic RNase inhibitor; IMP, inosine 5′ phosphate.

* Corresponding author. Tel.: +30 210 7273841; fax: +30 210 7273831.
E-mail address: ddl@eie.gr (D.D. Leonidas).

0223-5234/$ – see front matter © 2009 Elsevier Masson SAS. All rights reserved.
doi:10.1016/j.ejmech.2009.06.039

Table 1
Inhibition of BS-RNase and RNase A by pyridinyl phosphonucleotides at pH 6.0.

Inhibitor	K_i (μM)	
	BS-RNase	RNase A
U2′p	40.8 ± 3.4	11.6 ± 1.2
U3′p	63.2 ± 4.5	78.5 ± 1.3
UDP	1046.4 ± 50.2	647.0 ± 57.0
C3′p	27.9 ± 1.3	20.1 ± 1.4
C5′p	1557.9 ± 84.3	844.2 ± 92.4

The central region of the catalytic sites of BS-RNase and RNase A is conserved and like in RNase A is composed of different subsites that bind different parts of the RNA substrate. These subsites are noted as B, R, or P according to the part of the nucleotide they bind (base, ribose, or phosphate group, respectively) and a number which indicates their position with respect to the central subsite where the hydrolysis of the phosphodiester bond occurs (subsite P_1). BS-RNase, like all members of the RNase A superfamily, has strong specificity for pyrimidines at B_1 and prefers purines at B_2. Apart from the ribonuclease activity, another prerequisite for the BS-RNase antitumor function [11] is the dimeric structure that allows it to evade the potent cytoplasmic RNase inhibitor (cRI) when entering the cell [12].

BS-RNase has a potential for therapeutic applications against cancer since it permeates and destroys only malignant cells. Conjugation of BS-RNase with polymers decreases its proteolysis in bloodstream thereby enhancing its antitumor activity [13] while at the same time reduces its immunogenicity. Furthermore, BS-RNase attached to nanoparticles made of polylactic acid kills leukemia and lymphoma cell lines in vitro [14]. However, the antitumor action of BS-RNase is associated with severe side effects such as aspermatogenicity, immunosuppression and embryotoxicity [1,15–20] which together with other factors (bioavailability, cell permeability etc) render any potential pharmaceutical use of BS-RNase problematic [21]. To overcome some of these problems various attempts have been made to transfer some of the structural characteristics responsible for the antitumor action of BS-RNase to human pancreatic ribonuclease (HP-RNase) [22,23] or to RNase A [24–27] or to produce engineered forms of BS-RNase that may cause less side effects [28–30]. In order to enhance the potential benefits that these attempts might have once they reach their goal we propose the ancillary use of a potent and specific BS-RNase inhibitor which could play the role of an on/off switch acting as an antidote to the biological actions of BS-RNase. In this way, the attainment of a delicate balance between effective antitumor activity and side effect actions might be feasible. This way it might be possible to inhibit the biological activities of BS-RNase, including however its antitumoral action, when the side effects outweigh the beneficial anticancer action of BS-RNase threatening the patient's well-being. Such an approach will be assisting the other strategies which are outlined above, to overcome the side effects of the BS-RNase antitumor action. A similar strategy is applied successfully nowadays for the most widely used anticoagulant, heparin and its antidote protamine. Heparin, a highly sulfated glycosaminoglycan, is widely used as an injectable anticoagulant in cardiovascular surgeries but often leads to a high incidence of bleeding complications. Heparin activates the enzyme inhibitor antithrombin which in turn inactivates thrombin and other proteases involved in blood clotting; most notably factor Xa [31,32]. Protamine is used to reverse the anticoagulant action of heparin after cardiac or vascular surgeries [33] and more recently it has been used in aptamer-antidote pairs as reversible antagonists for coagulation factor IXa [34].

The high cost in the development of novel drugs has led nowadays to rational drug design approaches for the development of effective treatments to a variety of diseases. The efficiency of the rational drug design method relies mainly on the in-depth understanding of molecular activity, the amount of available experimental

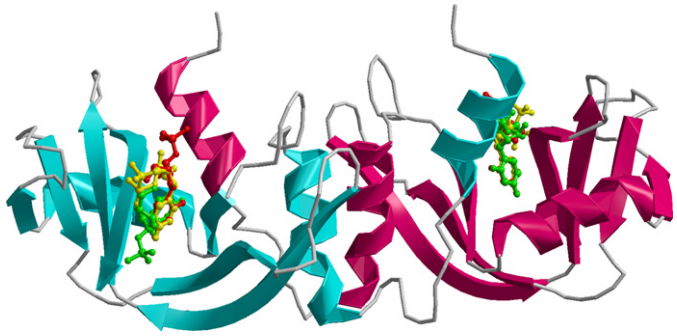

Fig. 1. A schematic representation of the BS-RNase molecule with the five inhibitor molecules superposed bound. Subunits SA and SB are coloured red and cyan, respectively.

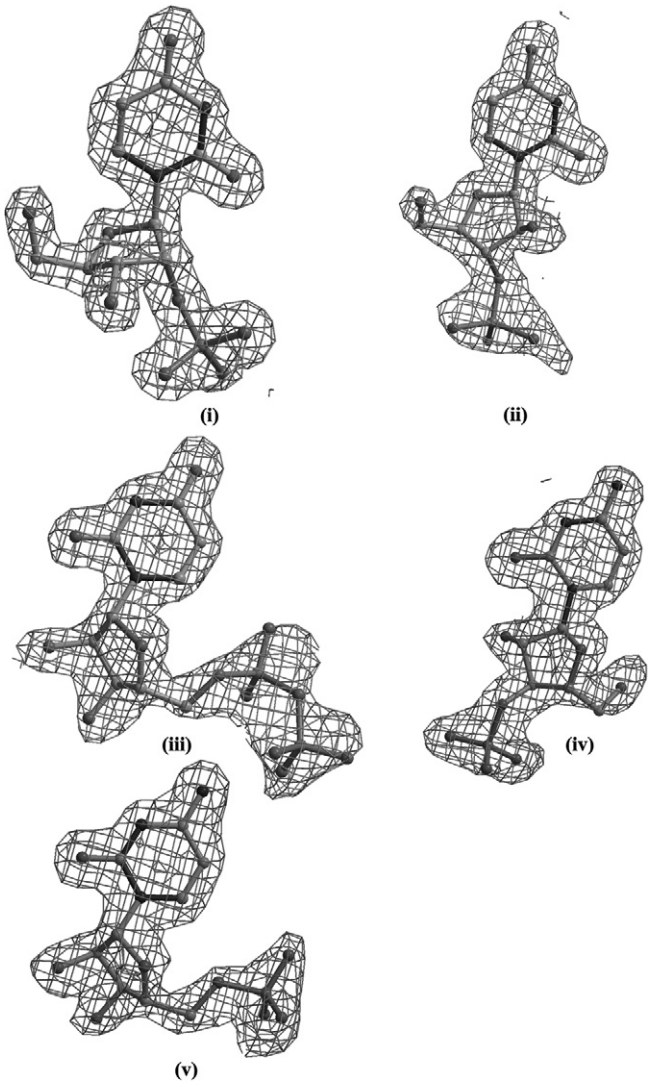

Fig. 2. Diagrams of the sigmaA 2|Fo|−|Fc| electron density maps calculated from the BS-RNase model before incorporating the coordinates of the ligand, are contoured at 1.0 σ level. The refined structures of the inhibitor are shown for U2′p (i), U3′p (ii), UDP (iii), C3′p (iv), and C5′p (v), respectively.

data, and the structural information about drug targets in complex with natural ligands. Although the crystal structure of BS-RNase has been reported sixteen years ago [35], only three BS-RNase-ligand complex structures have been studied so far. These ligands are all dinucleotides: 3′,5′-CpA [36], 2′,5′-UpA [37], 2′,5′-UpG [8] and their effect on the BS-RNase activity in the solution has not been studied. The initiation of a structure-assisted inhibitor design effort requires a significant number of BS-RNase – inhibitor complex structures to use as starting templates for further design and optimization. Since BS-RNase, like RNase A, has a higher affinity for pyrimidine than purine nucleotides [38], we have initiated our studies by analyzing the binding of five pyrimidinyl substrate analogues, uridine 2′ phosphate (U2′p), uridine 3′ phosphate (U3′p), uridine 5′ diphosphate (UDP), cytidine 5′ phosphate (C5′p), and cytidine 3′ phosphate (C3′p) by kinetic experiments and X-ray crystallography at high resolution. The impetus to initiate the efforts towards the design of potent small inhibitors with binding studies with simple phosphomononucleotides also stems from the general concept that in drug design good quality leads are those that allow faster optimization to candidate drugs i.e. have a molecular weight less than 250, which allows compound to "grow" during the optimization process, display moderate binding affinity (affinity will be added with growth) and contain polar groups which insure solubility, are reactive, and pick up hydrogen bonding interactions. These compounds are more amenable to modifications, have a moderate hydrophobicity/hydrophilicity profile and chemical complexity while they need less help to enter cells. The binding of mononucleotides will also provide data to map the active site on the degree of specificity of subsites such as B_1, R_1 and P_1 since the binding of small nucleotides to the enzyme is less constrained as opposed to the binding of dinucleotides whose binding mode is strongly guided by the architecture of the entire active site of the enzyme as well as their own chemical structure. Furthermore, the in depth mapping of the active site of BS-RNase through inhibitor binding studies can serve as a good working model for the general understanding of in vivo cellular RNA catalysts.

The five phosphonucleotide ligands, presented in this study, are competitive inhibitors of the enzyme with U2′p, U3′p and C3′p displaying K_i values in the μM range, bind at the active site of BS-RNase and their structural mode of binding suggests ways for further optimization through structure assisted rational design. We have also evaluated in vivo their potential to act as antidotes for the side-effects of the BS-RNase anticancer activity. In vivo studies on the aspermatogenic effect of BS-RNase in mice, after intratesticular injections of 10 μg of BS-RNase and inhibitors C3′p and C5′p, have shown that both inhibitors completely inhibit the biological action of BS-RNase in mice confirming our proposal.

Unfavourable adsorption, distribution, metabolism and excretion (ADME) properties can in many cases lead to the clinical trials failure of otherwise potentially successful drug candidates. Their evaluation, therefore, at an earlier stage is desired. Here we also present the predicted ADME properties of our inhibitors calculated using the QikProp program which estimates both physically significant descriptors and pharmaceutically relevant properties. Fulfillment, or not, of Lipinski's 'rule of five' [39,40], Veber and coworkers suggested properties for oral bioavailability [41], and the important physicochemical properties of solubility, polar surface area, permeability and lipophilicity are reported and analyzed.

2. Results and discussion

2.1. Kinetics

Since, inhibition constant values are strongly dependent on pH and ionic strength they can be only compared to RNase A inhibition constants measured under similar conditions. Thus, we measured the RNase A inhibition constants under the same conditions as we did for BS-RNase for U2′p, UDP, and C5′p while for U3′p and C3′p values existed in the literature [42]. The inhibition constants (K_i) of the inhibitors for BS-RNase and RNase A are listed in Table 1. All five nucleotides are competitive inhibitors of BS-RNase and RNase A. In both enzymes U2′p, U3′p, and C3′p are potent inhibitors with K_i

Table 2
Crystallographic statistics.

BS-RNase complex	U2′p	U3′p	UDP	C3′p	C5′p
Soaking conditions					
Ligand concentration (mM)	25	25	25	60	125
Soaking time (h)	24	24	30	24	24
pdb entry code	3DJO	3DJP	3DJQ	3DJV	3DJX
Resolution (Å)	27.7–1.60	27.7–1.60	25.2–1.53	27.6–1.60	27.8–1.70
Outermost shell	1.63–1.60	1.64–1.60	1.57–1.53	1.63–1.60	1.70–1.73
Reflections measured	512,176	330,505	880,739	300,876	310,907
Unique reflections ($F>0$)	31,871	31,948	35,718	29,510	25,228
R_{symm}[a]	0.066 (0.466)	0.041 (0.389)	0.043 (0.317)	0.036 (0.273)	0.059 (0.445)
Completeness (%)	99.9 (98.4)	99.8 (96.6)	97.5 (76.1)	97.9 (85.1)	98.1 (98.7)
Redundancy	5.9 (4.1)	4.8 (3.3)	6.3 (4.5)	4.9 (3.7)	3.9 (3.8)
$<I/\sigma I>$	12.4 (3.0)	19.0 (2.9)	21.4 (4.4)	26.2 (5.4)	14.1 (3.4)
R_{cryst}[b]	0.184 (0.229)	0.188 (0.243)	0.201 (0.213)	0.177 (0.193)	0.169 (0.199)
R_{free}[c]	0.226 (0.282)	0.229 (0.288)	0.233 (0.239)	0.204 (0.250)	0.204 (0.255)
No. of atoms per asymmetric unit	964	964	968	964	964
No. of solvent molecules	327	291	313	309	307
rms deviation from ideality					
In bond lengths (Å)	0.008	0.011	0.007	0.007	0.010
In angles (°)	1.2	1.5	1.1	1.3	1.3
Average B factor					
Protein atoms (Å^2) (mol A/B)	9.9/12.2	14.7/14.1	13.9/14.8	11.1/10.8	11.9/11.9
Solvent molecules (Å^2)	28.8	32.2	35.1	28.8	28.6
Ligand atoms (Å^2) (mol A/B)	14.3/16.7	29.4/28.2	34.9/35.7	25.0/27.0	22.5/23.3

[a] $R_{symm} = \Sigma_h\Sigma_i|I(h) - I_i(h)|/\Sigma_h\Sigma_i I_i(h)$ where $I_i(h)$ and $I(h)$ are the ith and the mean measurements of the intensity of reflection h.
[b] $R_{cryst} = \Sigma_h|F_o - F_c|/\Sigma_h F_o$, where F_o and F_c are the observed and calculated structure factors amplitudes of reflection h, respectively.
[c] R_{free} is equal to R_{cryst} for a randomly selected 5% subset of reflections not used in the refinement [106]. Values in parentheses are for the outermost shell.

values in the μM range while UDP and C5′p are low-moderate inhibitors with K_i values in the mM range. Both RNases show a preference for cytosine over uracil since the K_i values of C3′p inhibition are lower than those of the U3′p. Also they both show a preference for a 2′ phosphate group than a 3′ phosphate, while the preference for either the 2′ or the 3′ phosphate group is much stronger than the preference for a 5′ phosphate or diphosphate group. A relative comparison of the K_i values for RNase A and BS-RNase shows that the five inhibitors, with the exception of the first two (C3′p and U2′p), follow the same potency pattern in the two enzymes. Thus, in BS-RNase the order of potency is C3′p > U2′p > U3′p > UDP > C5′p, while in RNase A is U2′p> C3′p>

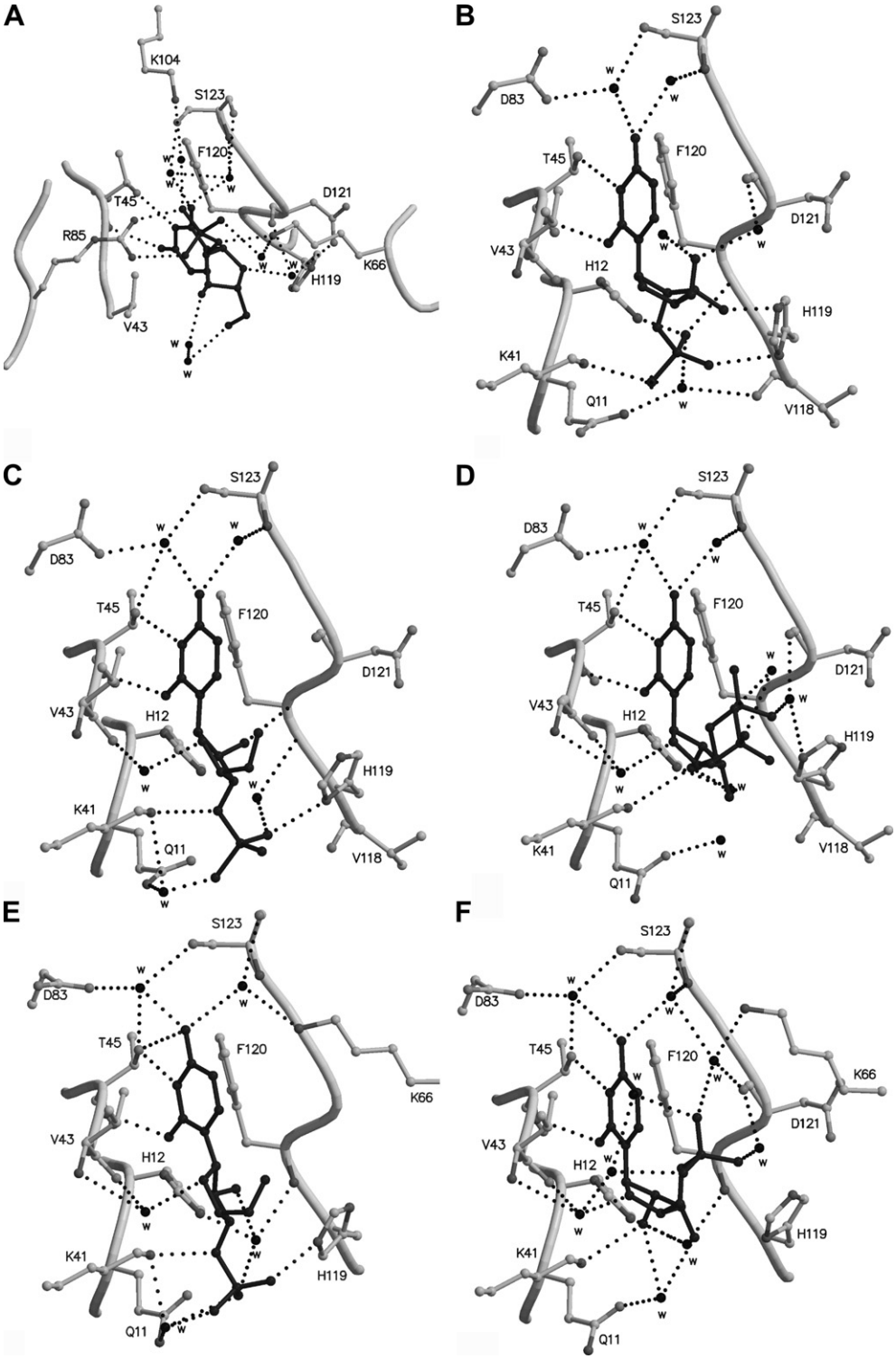

Fig. 3. (A, C, D, E, and F) Diagrams of the interactions between BS-RNase subunit SA and U2′p, U3′p, UDP, C3′p, and C5′p, respectively. (B) Diagram of the interactions between BS-RNase and U2′p in subunit SB. Residues are drawn as ball-and-stick models and water molecules are shown as black spheres labelled with letter "w". Hydrogen bonds are indicated as dashed lines.

U3′p > UDP > C5′p. Overall, all five inhibitors are more potent for RNase A than for BS-RNase A with the exception of C3′p which displays a similar potency against the two enzymes.

2.2. Overall structures

Although the crystallization experiment was carried out on native protein solutions which contain two quaternary forms (M × M and M = M) of BS-RNase only the swapped dimer (M × M) exists in the crystal. The hinge peptide region (residues 16–22) is well defined within the 2Fo–F_c electron density map for both subunits SA and SB. The sigmaA weighted F_o–F_c and $2F_o$–F_c electron density maps of the complex structures clearly indicated binding of one inhibitor molecule at each of the two subunits of the BS-RNase dimer (referred as SA and SB hereafter) (Fig. 1). All atoms of the inhibitors are clearly defined within the electron density map (Fig. 2) and have temperature factors similar to those of the protein (Table 2). The rms distances between the structures of free BS-RNase [35] and those of the liganded complexes are 1.16 Å, 1.04 Å, 1.06 Å, 1.09 Å, and 1.11 Å for 248 equivalent Cα atoms of the free BS-RNase and U2′p, U3′p, UDP, C3′p, and C5′p complexes, respectively. Structural comparison of the free and the complexed structures reveals that the binding of the inhibitors induces conformational changes to the quaternary protein structure and the protein structure is slightly more compact in the complexed than in the free structure. This is apparent when comparing the position of the relative position of the two subunits SA and SB that comprise the structure of BS-RNase in the free and in the liganded form. Superimposition of the two structure forms reveals that the two subunits rotate with respect to each other pivoting on the interchain disulfide bridges that link Cys31 and Cys32 of SA to Cys31 and Cys31 of SB, respectively, and in the complexed structure approach each other by approximately 1.0 Å. Similar variations have been observed upon ligand binding in all previous BS-RNase complex structures [8,36,37] and are characteristic of the flexibility of this enzyme. The structures of the U2′p, U3′p, and C3′p complexes are refined at 1.6 Å resolution, while those of UDP, and C5′p complexes are defined at 1.5 Å and 1.7 Å resolution, respectively.

In all free RNase A and BS-RNase structures reported so far [35,43] the side chain of the catalytic residue His119 adopts two conformations denoted as A ($\chi_1 = \sim 160^\circ$) and B ($\chi_1 = \sim$approximately -80°), which are related by a 100° rotation about the Cα–Cβ bond and a 180° rotation about the Cβ–Cγ bond [35,44–47]. These conformations in RNase A are dependent on the pH [48] and the ionic strength of the crystallization solution [49]. Like in all the previously studied BS-RNase–ligand complexes [8,36,37], His119 in all five complex structures reported here adopts conformation A with $\chi_1 = \sim 160^\circ$, in both molecules of the BS-RNase homodimer.

2.3. The binding of U2′p and U3′p to BS-RNase

The conformation of the phosphouridine in U2′p and U3′p, when bound at the active site, is similar in both complexes (Fig. 3A and B). The glycosyl torsion angle is at the anti conformation in both ligands, while the backbone and phosphate torsion angles have values that are common for protein-bound nucleotides [50]. The only exception is the conformation of the ribose in U2′p which adopts the unusual *O4′-endo* conformation, while in U3′p adopts the commonly found [50] *C3′-endo* conformation (Table 3).

The inhibitor binding mode for U3′p is similar in both active sites of the BS-RNase homodimer. Thus, the uracil is bound in the pyrimidines preferring subsite B_1, where it forms hydrogen bond interactions with the main and side chain atoms of Thr45. The rest of the U3′p molecule binds with the ribose at R_1 and the phosphate group in subsite P_1 where it forms hydrogen bonds with residues Gln11, His12, Lys41 and His119 (Table 4, Fig 3C). The binding mode of U2′p differs in the two active sites of the BS-RNase dimer. Although in both protein subunits, the uracil binds at B_1 and engages in hydrogen bond interactions with Thr45; its orientation differs by 120°. In subunit SA the ribose and the phosphate group are not in R_1 and P_1, respectively, but the inhibitor molecule is oriented towards the surface of the protein molecule (Fig. 3B)

Table 3
Torsion angles for inhibitors when bound to BS-RNase.

Inhibitor	U2′p		U3′p		UDP		C3′p		C5′p	
BS-RNase subunit	SA	SB	SA	SB	SA	SB	SA	SB	SA	SB
Backbone torsion angles										
O5′–C5′–C4–C3′ (γ)	45 (+*sc*)	57 (+*sc*)	95 (+*ac*)	66 (+*sc*)	107 (+*ac*)	128 (+*ac*)	88	76	76	80
C5′–C4′–C3′–O3′ (δ)	83 (+*sc*)	77 (+*sc*)	125 (+*ac*)	127 (+*ac*)	100 (+*ac*)	100 (+*ac*)	113	109	103	89
C5′–C4′–C3′–C2′	−159	−162	−127	−125	−139	−139	−130	−131	−144	−155
C4′–C3′–C2′–O2′	−72	−63	130	130	−105	−105	148	147	−91	−83
Glycosyl torsion angle										
O4′–C1′–N1–C2 (χ′)	−163 (anti)	−154 (anti)	−150 (anti)	−143 (anti)	−147 (anti)	−148 (anti)	−114 (anti)	−107 (anti)	−157 (anti)	−156 (anti)
Pseudorotation angles										
C4′–O4′–C1′–C2′ (ν_0)	6	9	−8	−8	−4	−8	43	40	7	−3
O4′–C1′–C2′–C3′ (ν_1)	−31	−36	4	6	−6	−3	−46	−43	−19	−18
C1′–C2′–C3′–C4′ (ν_2)	42	48	1	−2	13	12	31	31	23	31
C2′–C3′–C4′–O4′ (ν_3)	−40	−44	−6	−2	−16	−18	−8	−9	−20	−34
C3′–C4′–O4′–C1′ (ν_4)	22	22	8	7	12	16	−21	−18	8	23
Phase	11 (C3′-endo)	8 (C3′-endo)	83 (O4′-endo)	105 (O4′-endo)	33 (C3′-endo)	47 (C4′-exo)	332 (C2′-exo)	334 (C2′-exo)	84 (O4′-endo)	12 (C3′-endo)
Phosphate torsion angles										
C4′–C3′–O3′–P1 (ε)			−118 (−*ac*)	−120 (−*ac*)			−102	−101		
P1–O3′–C3′–C2′			128	128			143	143		
C4′–C2′–O2′–P1 (ε′)	−136 (−*ac*)	−118 (−*ac*)								
P1–O2′–C2′–C1′	152	170								
O3A–PA–O5′–C5′ (α)					−102 (−*ac*)	−96 (−*ac*)			68	50
PA–O5′–C5′–C4′ (β)					−138 (−*ac*)	−138 (−*ac*)			179	177

Definitions of the torsion angles are according to the current IUPAC-IUB nomenclature [107], and the phase angle of the ribose ring is calculated as described previously [108].

engaging in hydrogen bond interactions with water molecules and with the side chain atoms of Arg85 (Table 4). In BS-RNase subunit SB the ribose and the phosphate group of U2′p are bound in R_1 and P_1, respectively (Fig 3A), like in the U3′p complex. In RNase A, Arg85 is the sole component of subsite P_{-1} that accommodates the phosphate of a nucleotide bound in B_3 (Gln69) [51]. The existence of this subsite in RNase A has been inferred by mutagenesis experiments [52] and has been observed in structural studies [53]. In RNase A replacement of Arg85 by an alanine increases the Km for poly(cytidylic acid) more than 15 times with respect to the native enzyme [52]. In the RNase A–IMP complex, the side chain of Arg85 is at a hydrogen-bonding distance from the 5′ phosphate group of an IMP molecule which has its ribose bound at subsite B_3 [53]. The structural equivalent of this residue in BS-RNase is also Arg85. Since in subunit SA the 2′phosphate of U2′p is also in a hydrogen bond distance from the side chain of Arg85 and its ribose is bound at B_3, for the first time, we have direct evidence for the structural conservation of this subsite in BS-RNase.

Both ligands, U2′p and U3′p, also engage in a network of water mediated polar interactions with the protein. Thus, in both subunits SA and SB the uracil of U2′p is involved in a water-mediated polar interaction network with Asp83 and Ser123, the ribose with His12, Val43, Val118, His119, and Phe120, and the phosphate with Lys104 and Ser123. In subunit SA, the uracil of U3′p is involved in water-mediated interactions with Asp83 and Ser123, the ribose with Val43, Asn67, His119, and Asp121, and the phosphate with Gln11, His12, Lys41, and His119. In subunit SB water molecules are conserved between the complex structures of U2′p and U3′p and hence U3′p is involved in similar water-mediated polar interactions as U2′p.

On binding at the BS-RNase active site, U2′p and U3′p molecules become buried and participate in a total of 53 and 41 van der Waals interactions with 16 and 13 different BS-RNase residues in the two protein subunits, respectively. The solvent accessibility of the free U2′p molecule is 440 Å^2. This area reduces to 164 Å^2 and 126 Å^2, when U2′p binds to subunits SA and SB of the BS-RNase homodimer, respectively; indicating that 63% and 71% of the U2′p surface becomes buried upon binding. The greatest contribution comes from the polar parts of the ligand that contribute 81% of the surface, which becomes inaccessible for the ligand in subunit SA, whereas for the ligand in protein subunit SB the non-polar parts contribute 73% of the inaccessible surface. Molecule U3′p has a solvent accessible area of 453 Å^2. Upon binding to BS-RNase subunits SA and SB, this area reduces to 152 Å^2 and 162 Å^2, respectively. The polar parts of the ligand contribute the most in this reduction as they cover 67% and 70% of the ligand surface which becomes inaccessible upon binding to BS-RNase subunits SA and SB, respectively.

2.4. The binding of UDP to BS-RNase

The conformation of the bound ligand is very similar in both active sites of the BS-RNase homodimer. The glycosyl torsion angle is at the *anti* conformation while the backbone and phosphate

Table 4
Potential hydrogen bonds of inhibitors with BS-RNase in the crystal.

Inhibitor atom	BS-RNase	Distance (Å)									
		U2′p		U3′p		UDP		C3′p		C5′p	
		SA	SB	SA	SB	SA	SB	SA	SB	SA	SB
N3	Thr45 Oγ1	2.7	2.7	2.7	2.7	2.7	2.7	2.7	2.7	2.7	2.7
N4	Thr45 Oγ1							3.2	3.1		
O2	Thr45N		2.9	2.9	2.9	2.9	2.9	2.9	3.0	2.8	2.8
O4	Thr45N	2.9									
O2′	Lys66 Nζ	2.8									
O2′	Lys41 Nζ					3.1	3.1			2.9	2.8
O2′	Phe120 O			2.3	2.3						
O3′	His119 Nϵ2		2.2								2.9
O3′	Lys41 Nζ			3.0				2.9			
O1A	Arg85 Nη1	2.7									
O1A	His119 Nδ1		2.8	2.8							
O1A	His119 Nϵ2							2.9			
O2A	Gln11 Nϵ2		2.6								
O2A	Lys41 Nζ		2.9								
O3A	Arg85 Nη2	2.5									
O3A	His12 Nϵ2		2.5								
O3A	Phe120N		2.9								
N4	Water							3.2	3.0	2.9	3.0
N4	Water							2.9	2.8	3.1	3.2
O2	Water	2.5									
O4	Water		2.8	2.8	2.7	2.9	2.9				
O4	Water		2.7	2.9	2.9	2.9	2.9				
O2′	Water				3.1	2.7	2.6	3.1	3.1	2.8	2.7
O2′	Water									3.0	2.5
O4′	Water	3.0		3.1		3.0	3.0	3.2	3.2	2.9	2.4
O4′	Water										3.1
O5′	Water	2.9	2.7				2.7				
O5′	Water		2.9						2.9		
O3′	Water	2.7			2.7					3.2	2.9
O3′	Water									3.1	2.6
O1A	Water			2.8	2.6					2.7	
O2A	Water	2.8		2.2		2.8	3.1	2.6		2.8	2.4
O3A	Water		3.1		2.6	2.7	3.0	3.2	3.2	3.1	
O3A	Water	3.0						3.2	2.5	2.7	
O3A	Water	2.7									
O2B	Water					2.9	3.1				

Hydrogen bond interactions were calculated with the program HBPLUS [109].

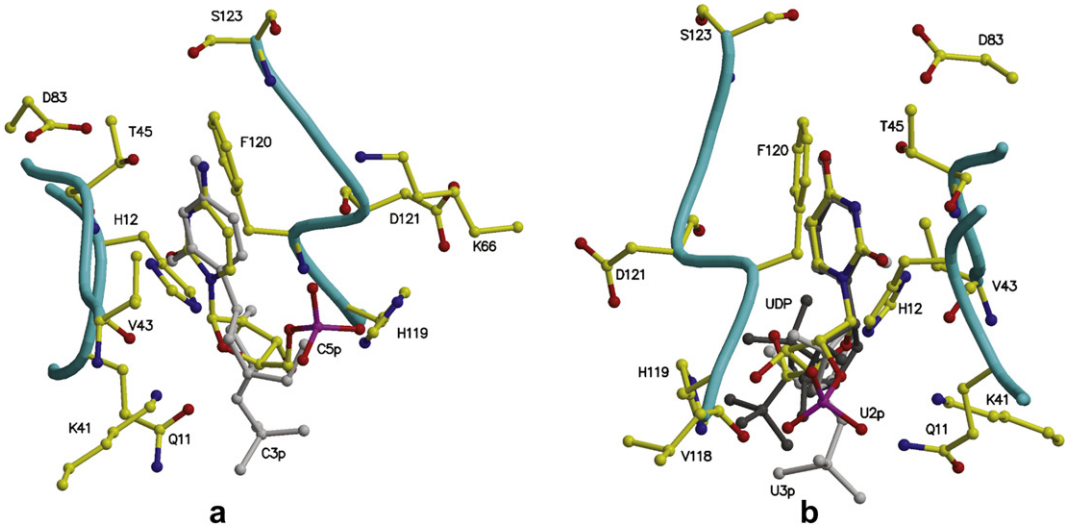

Fig. 4. (a) A schematic representation of BS-RNase subunit SA in complex with C5′p (coloured) in the active site. The inhibitor C3′p (in grey) is also shown superposed. (b) A schematic representation of BS-RNase subunit SB in complex with U2′p (coloured) in the active site. The inhibitors U3′p (in grey) and UDP (in green) are also shown superposed.

torsion angles have values that are usually found in protein-bound nucleotides [50]. The only exception is the conformation of the ribose which adopts the unusual [50] *C4′-exo* conformation in the ligand bound in BS-RNase SB while at the other subunit is at the C3′-*endo* conformation (Table 3).

The inhibitor binds similarly in both active sites, with the uracil in subsite B_1 taking part in hydrogen bond interactions with Thr45 and in water mediated interactions with atoms from Ser123 and the side chain of Asp83. The pyrophosphate group is away from the phosphate recognition subsite P_1 and points towards the solvent (Fig. 3D, Table 4). Water molecules are conserved in the active site of SA and SB, creating a similar network of water-mediated interactions between UDP and protein residues. Thus, atom O4 of the uracil participates in a water-mediated network of polar interactions with Asp83, Lys104, and Ser123. The ribose of UDP is involved in water-mediated interactions with Gln11, His12, Val43, His119, and Phe120. The pyrophosphate atoms form hydrogen bond interactions with three water molecules (Table 4). Two of them are at the surface of the protein molecule and the third mediates interactions with Asp121. UDP participates in a total of 19 and 24 van der Waals interactions with 7 and 8 different BS-RNase residues in the two protein subunits, respectively. The solvent accessibility of the free UDP molecule is 490 Å^2. Upon binding to BS-RNase this area reduces to 212 Å^2 indicating that 57% of the UDP surface becomes buried. The greatest contribution comes from the non-polar parts of the ligand that cover 85% of the surface, which becomes inaccessible.

2.5. The binding of C3′p and C5′p to BS-RNase

The conformation of C3′p differs from that of C5′p as indicated by differences in their torsion angle values (Table 3) and hence their binding mode to BS-RNase differs (Fig. 3E and F). Superposition of the C3′p complex onto the C5′p complex reveals that the two ring planes of the cytosine in B_1 have an inclination of 15°. Despite this difference, in both complexes and in SA and SB, the cytosine forms hydrogen bond interactions with Trh45 and it is involved in water-mediated interactions with Asp83, and Ser123 (Table 4). The ribose of C3′p adopts the rather unusual *C2′-exo* conformation, while that of C5′p is in two different conformations (*O4′-endo* and *C3′-endo*) in SA and SB, respectively (Table 3, Fig. 3E). In the C3′p complex in subunit SA the ribose participates in water-mediated hydrogen bond interactions with His12 and Val43. In subunit SB the ribose forms water-mediated hydrogen bond interactions with residues His12, His119, and Phe120. The ribose of C5′p, in both subunits SA and SB, is involved in a water-mediated hydrogen bond network with Gln11, His12, Val43, and Phe120. The phosphate group of C3′p binds in P_1 and forms hydrogen bonds with atoms from residues Gln11, Lys41, and His119 (Table 4) in both subunits SA and SB. In subunit SA is involved in water-mediated interactions with residues Gln11, His12, Lys41, and Phe120 but in subunit SB only with Gln11. In the C5′p complex, the phosphate group does not bind in P_1 but it is oriented towards P_0 (the closest distance of the phosphate

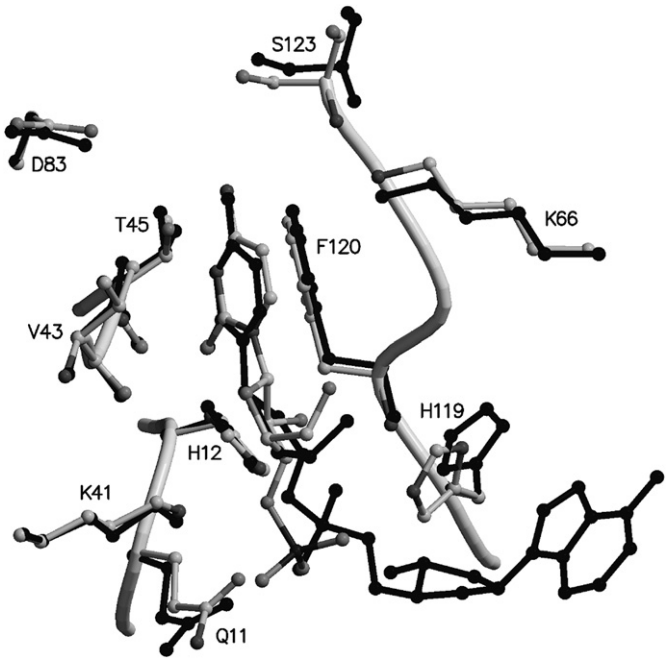

Fig. 5. Structural comparisons of the BS-RNase–C3′p complex (grey) and BS-RNase–C3′,5′A (black) in subunit SA.

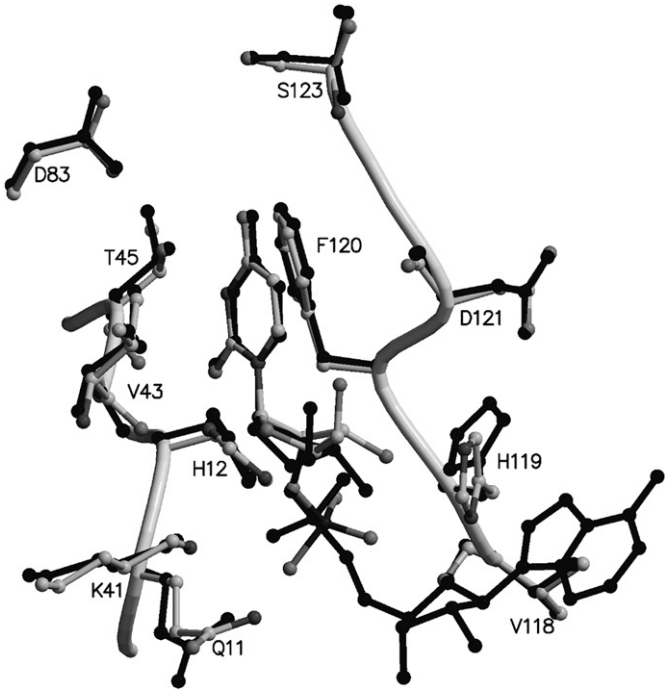

Fig. 6. Structural comparisons of the BS-RNase–U2′p complex (grey) and BS-RNase–U2′,5′A (black) in subunit SB.

group from atoms of the side chain of Lys66, the sole component of this subsite, is 4.8 Å). In this position, in subunit SA, two water molecules mediate interactions between the phosphate oxygens and residues Lys66, and Asp121, while in subunit SB the phosphate form a hydrogen bond with a single water molecule which does not mediate any interactions with protein residues.

On binding at the BS-RNase active sites, C3′p and C5′p molecules become buried and participate in a total of 48 and 52 van der Waals interactions with 13 and 14 different BS-RNase residues in the two subunits, respectively. The solvent accessibility of the free C3′p molecule is 455 Å^2. This area reduces to 138 Å^2 (SA) and 144 Å^2 (SB) in the BS-RNase–C3′p complex, indicating that 70% and 68% of the C3′p surface becomes buried upon binding. The greatest contribution comes from the polar parts of the ligand that cover 81% of the surface, which becomes inaccessible for the ligand in both subunits. Molecule C5′p has a solvent accessible area of 445 Å^2. Upon binding to BS-RNase, this area reduces to 153 Å^2 and 170 Å^2 in subunits SA and SB, respectively. The polar parts of the ligand contribute the most in this reduction as they cover 53% and 63% of the ligand surface which becomes inaccessible upon binding to BS-RNase subunits SA and SB, respectively.

2.6. SAR analysis

The pyrimidine binding subsite B_1 is conserved between RNase A and BS-RNase. The binding modes of U3′p, C3′p, and U2′p (subunit SB) in BS-RNase are similar to those observed in RNase A [54,55]. However, as noted above the binding mode of U2′p in subunit SA is quite different from that in subunit SB (Fig. 3A and B) and different from that of U2′p in RNase A [54]. Thus, only the uracil plane of U2′p superposes in the two complexes, while the rest of the ligand is oriented towards different directions.

The interactions of 3′,5-CpA [36] 2′,5′-UpA [37], and 2′,5′-UpG [8] with BS-RNase have been examined by X-ray crystallography. The interactions between BS-RNase and the cytosine (Fig. 4a) or uridine (Fig. 4b) of the five inhibitors are similar to those observed for the pyrimidines of 3′,5′-CpA and 2′,5′-UpA in their respective complexes with BS-RNase [36,37] indicating the strong specificity of subsite B_1 (Figs. 5 and 6). However, subsites R_1 and P_1 do not show the same degree of specificity since the binding modes of the ribose and the phosphate group varies between the dinucleotide and the mononucleotide complexes (Fig. 4). Only U3′p, U2′p, and C3′p follow the same binding pattern with 3′,5′-CpA and 2′,5′-UpA (Figs. 5 and 6). C5′p and UDP bind quite different from these two dinucleotides since their phosphate groups are away from subsite P_1. The C5′p and UDP binding modes do not resemble the binding mode of 2′,5′-UpG [8] which binds in the retro-binding mode observed for RNase A [56]. Furthermore and despite the fact that we used rather high concentration (60 and 125 mM) for C3′p and C5′p, we did not observe any binding at the potential allosteric site of BS-RNase which is located at the interface of the two subunits SA and SB and where 2′,5′UpG also binds [37].

It seems that the diversity in the structural skeleton of the inhibitors has a significant impact on BS-RNase inhibition. Although comparison of k_{cat}/K_m values for cytidylyl and uridylyl substrates has previously [57] led to the proposal that the B_1 site of RNase A has a small preference for cytidylyl over uridylyl substrates this is not evident when comparing the K_i values of cytidylyl and uridylyl mononucleotide inhibitors (Table 1). It seems that in the phosphomonoculeotide inhibitors the binding of the phosphate groups dominates their potency, as has been seen previously [54,58]. The primary functional component of the B_1 subsite is Thr45, which forms two hydrogen bonds with pyrimidines: its main-chain NH donates a hydrogen atom to O2 of either base, and its Oγ1 can donate to N3 of cytosine or accept from N3 of uracil. Thus the preference of both BS-RNase and RNase A for cytidine versus uridine would imply that the hydrogen bond between the pyrimidine O2 and Thr45 NH is stronger for cytosine and cytosine O2 should carry a larger partial negative charge, making it a better hydrogen acceptor. Cytosine might also engage in more favorable stacking interactions with Phe120 due to the greater delocalisation of electrons throughout its ring [59].

Table 5
The effect of C3′p or C5′p on the aspermatogenic activity of BS-RNase in mice.

Substances injected in μg/mouse	No. of mice	Index weight of testes ± SEM		Width of spermatogenic layers ± SEM		Diameter of somniferous tubules ± SEM	
		Injected testes	Non-injected testes	Injected testes	Non-injected testes	Injected testes	Non-injected testes
PBS (control)	5	43 ± 7	40 ± 7	61 ± 7	63 ± 8	151 ± 5	152 ± 9
BS-RNase 10 μg	5	40 ± 5	42 ± 4	23 ± 6^{++}	61 ± 7	134 ± 6^{++}	153 ± 5
BS-RNase + C3′p (1:1)[a]	5	51 ± 2	51 ± 7	66 ± 5	62 ± 6	159 ± 4	154 ± 5
BS-RNase + C3′p (100:1)[a]	11	20 ± 6^{++}	41 ± 5	34 ± 10^{++}	65 ± 8	140 ± 8^{+}	159 ± 4
BS-RNase 1 + C5′p (1:1)[a]	5	51 ± 1	44 ± 3	64 ± 4	62 ± 7	165 ± 7	156 ± 6
BS-RNase + C5′p (100:1)[a]	9	31 ± 9^{+}	43 ± 6	51 ± 5^{+}	65 ± 5	133 ± 6^{++}	163 ± 6

$^{+}P < 0.05$, $^{++}P < 0.01$.
[a] Ratios are w/w.

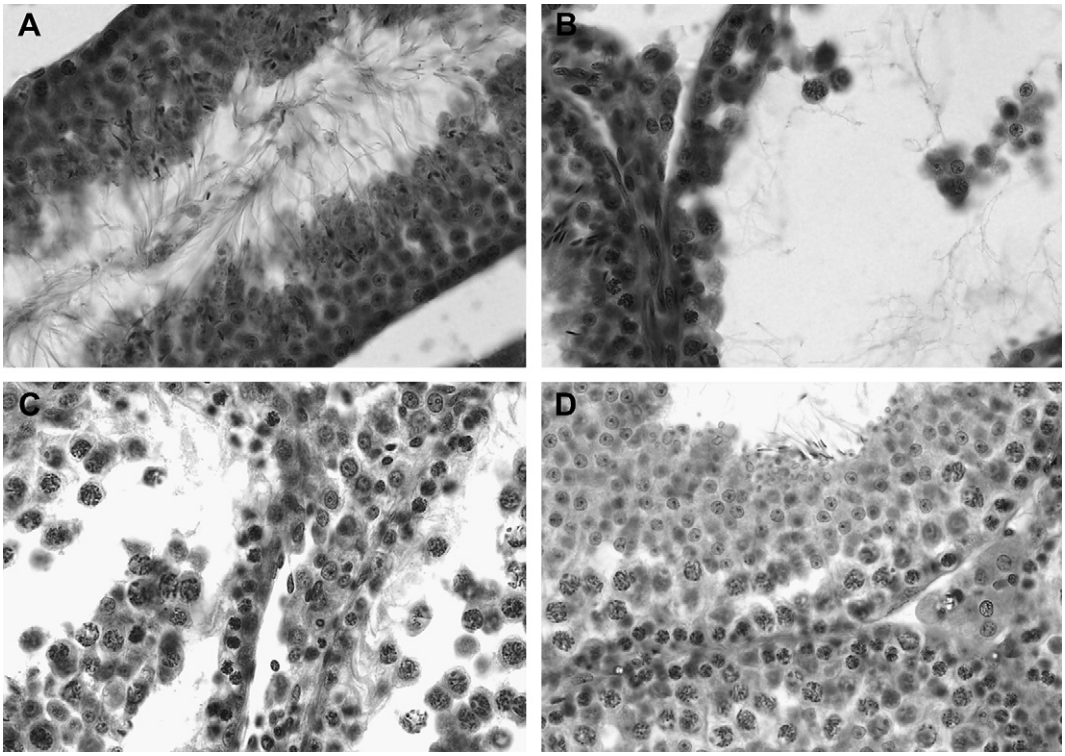

Fig. 7. (A) The control picture in which no spermatogenic cells are degenerated in sperm tubule. Spermatogonia, primary and secondary spermatocytes, spermatids and sperms inside of tubule of testis are visible. (B) The testicular tissue with spermatogenic cells in mice injected with a mixture of BS-RNase and C3′p in ratio 100:1 (w/w) is destroyed fully in spermatogenic tubules. Most of the testicular tissue cells lacked order with the exception of spermatogenic cells and also partly of Sertoli cells. (C) Chaotic disorder of the testicular tissue and spermatogenic cells in mice injected with a mixture of BS-RNase and C5′p in a ratio of 100:1 (w/w). Only spermatogonia are presented near basal membrane. Sertoli cells are presented together with primary and secondary spermatocytes while some cells are mitotically active. (D) The spermatogenic cells in mice injected with a mixture of BS-RNase and C3′p in the ratio 1:1 (w/w). The width of the layer is in order.

BS-RNase has a preference for cytidine 3′ phosphate versus cytidine 5′ phosphate and uridine nucleotides. It seems that this is mainly due to the interactions of the phosphate group of the ligand with the protein residues in subsite P_1 and to a lesser extend to the preference of BS-RNase for cytidine versus uridine. This dominant role of the phosphate binding to the inhibition potency is more profound when comparing C3′p to C5′p. C3′p binds with the 3′ phosphate group at P_1 whereas C5′p binds with its C5′ phosphate group away from P_1 (Fig. 3E and F) and as a result C3′p is 10 times more potent than C5′p (Table 1). U2′p has its phosphate group at P_1 but only in SA. However this is enough to compensate for the preference of BS-RNase for cytidine over uridine and U2′p is 3 times more potent than C5′p (Table 1). The preference of the enzyme for cytidine versus uridine is pronounced in the cases of C3′p and U3′p where both ligands have their phosphate group at P_1 and C3′p is 2 times more potent than U3′p. Unexpectedly UDP, which has two phosphate groups, fails to place any of them in P_1 and as a result UDP is the less potent inhibitor of the other two uridilyl nucleotides.

2.7. In vivo experiments

Table 5 summarizes the results on the effect of C3′p and C5′p on the aspermatogenic activity of BS-RNase. The common dose (10 μg) used in the in vivo studies of BS-RNase [60] alone has a profound reduction in the width of spermatogenic layers and in the diameter of seminiferous tubules but not to the index weight of mice testes with respect to the non-treated testes or to control with PBS. This reduction is indicative of the degeneration of spermatogenesis caused by BS-RNase. When BS-RNase was injected as a mixture together with either C3′p or C5′p in a ratio of 1:1 (w/w) this degeneration was not evident showing that the inhibitors are capable to inhibit the aspermatogenic action of BS-RNase in vivo (Fig. 7). However, using a ratio of BS-RNase:inhibitor 100:1 (w/w) did not have any effect on the aspermatogenic action of BS-RNase (Fig. 7) indicating that among others a significant improvement in the potency of these inhibitors for BS-RNase is required so that small doses can have an effect in vivo. Nucleoside analogues have proven to be excellent agents for anticancer and antiviral therapy [61]. Effective doses in experiments in vivo range from 20 mg/kg/day to 100 mg/kg/day [62,63] to animals or 100–200 mg/m^2 in clinical trials [64]. Such as the doses used in the in vivo experiments with BS-RNase were within the limits of the effective concentrations of nucleosides used in anticancer and antiviral therapy.

Table 6
Application of Lipinski's 'Rule of 5' to our ligand test set[a].

Ligand	MW	No. H-bond acceptors[b]	No. H-bond donors[b]	log P (oct/wat)	Lipinski violations
C3′p	323.2	*14.1*	*6*	−2.063*	2
C5′p	323.2	*14.1*	*6*	−1.686	2
U2′p	324.2	*13.6*	5	−1.803	1
U3′p	324.2	*13.6*	5	−1.806	1
UDP	404.2	*15.6*	3	−1.704	2
Range 95% known drugs[c]	130.0–725.0	2.0–20.0	0.0–6.0	−2.0 to 6.5	–

[a] See text for full description. Lipinski violations are highlighted in italics. Predicted properties outside the range for 95% of known drugs are highlighted with an asterisk (*). All properties calculated using QikProp.
[b] Averaged over a number of configurations.
[c] Reference (QikProp version 3.1, U.M.).

Table 7
Other calculated ADME properties[a].

Ligand	Rotable bonds	Caco-2 permeability	QPlogS	QPlogKhsa	PSA	FISA	QPlogBB
C3′p	8	0	−1.587	−1.499	188.0	353.6*	−3.133*
C5′p	8	0	−1.388	−1.347	178.6	303.6	−2.4
U2′p	7	0	−1.399	−1.384	193.7	343.1*	−2.724
U3′p	7	0	−1.496	−1.453	190.7	338.0*	−2.818
UDP	10	0	−0.662	−2.084*	234.4*	386.9*	−3.571*
Range 95% known drugs[b]	0–15	<25 poor; >500 good	−6.5 to 0.5	−1.5 to 1.5	7.0–200.0	7.0–330.0	−3.0 to 1.2

[a] Calculated using QikProp (QikProp, version 3.1). Properties and descriptors with QPlogS (log *S*) representing predicted aqueous solubility (S in mol dm^{-3}); PSA, the van der Waals surface area ($Å^2$) of polar N and O atoms; QPlogBB (log BB), the predicted blood/brain barrier coefficient; FISA, the hydrophilic contribution ($Å^2$) to the SASA (SASA on N, O and Hs on heteroatoms); QPPCaco (PCaco), the predicted Caco-2 cell permeability (nm/s). Property values outside the range for 95% of known drugs are highlighted with an asterisk (*).
[b] Reference (QikProp version 3.1, U.M.).

2.8. ADME property prediction

Results from the QikProp ADME predictions are presented in Tables 6 and 7. Forty-four different properties consisting of principal descriptors and physiochemical properties were calculated. The most important of these are listed in the tables, together with those for which the property predictions are outside the ranges observed for 95% of known drugs (QikProp, version 3.1, U.M). If the predicted value for a property/descriptor was outside the training set range, it is flagged with an asterisk (*) in the tables.

As a first test of the drug-likeness of the ligands, we applied Lipinski's rule of 5 (Table 6) requiring candidates to have no more than 5 and 10 hydrogen bond donors and acceptors, respectively, molecular weights (MW) less than 500 amu, and partition coefficients between octanol and water (QPlog P(oct/wat)) less than 5. An orally active compound/drug should have no more than one violation of these rules. Only U2′p and U3′p with the maximum allowed violation of 1 (QPlogP(oct/wat) in each case) passed the Lipinski screening test. Poor absorption or permeation are more likely when a ligand molecule violates Lipinski's rule of 5 which is confirmed by the predicted Caco-2 cells permeability – used as a model for the gut–blood barrier [65,66] – which was 0 for all ligands. The main problem according to Lipinski's theory is an excess of H-bond acceptors for all ligands. Also, the QPlogP(oct/wat) values as a measure of lipophilicity are only theoretically valid for unionized species. However, reduced polar surface area correlates better with increased permeation rate than does lipophilicity [41,67,68] and is therefore an attractive alternative model for the prediction of oral drug absorption.

Vebers' study [41] on oral bioavailability suggested that a candidate's flexibility, measured as the number of rotable bonds (<10), and polar surface area (<140 $Å^2$) could be used as an early stage filter in drug design, although more recently it has been highlighted that this approach needs to be treated with caution with respect to choice of descriptor algorithm used and also because other factors can have significant influence on bioavailability [69]. With respect to the polar surface area criterion, however, a total sum of H-bond donors and acceptors criterion (≤12) can be used instead which is algorithm independent [41]. For our inhibitors set, all but UDP have a number of rotable bonds <10, but all ligands are much too polar irrespective of algorithm, or whether measured as sum of H-bond donors/acceptors (18.6–20.1) or PSA (178.6–234.4 $Å^2$). Indeed, the hydrophilic surface area (FISA), for four (338.0–386.9 $Å^2$) of our five inhibitors (C5′p excepted) exceeds the range observed for 95% of drugs (7.0–330.0 $Å^2$).

The aqueous solubility of a drug candidate is also a crucial property for its bioavailability [70], and given their excess polarity, all ligands are satisfactory with respect to their QPlogS values. QPlogKhsa is the prediction of binding to human serum albumin and all inhibitors except UDP (−2.084) lie within the expected range for 95% of known drugs (−1.5 to 1.5). The QPlogBB(brain/blood) barrier coefficient is satisfactory for C5′p, U2′p, and U3′p.

Of the 44 total QikProp descriptors, 3 ligands had one property value (C5′p (dipole moment), U2′p (FISA), U3′p (FISA)) outside the range for 95% of drugs. C3′p (FISA, QPlogP(oct/wat), QPlogBB) and UDP (FISA, PSA, QPlogKhsa, QPlogBB) were less promising with 3 and 4 property outliers, respectively. With the exception of C5′p, the inhibitors have hydrophilic (polar) surface areas which are too large, while C5′p's predicted dipole moment (16.1 Debye) is too high (95% of drugs range: 1.0–12.5 Debye). All ligands have too many H-bond acceptors according to Lipinski. In summary, for potential drug development using these ligands as scaffolds, the polar surface area/H-bond acceptor property values need to be significantly reduced. Reduced polar surface area will correlate with increased permeation rate with a threshold permeation rate imperative for oral bioavailability [41,67,68].

3. Conclusion

In the current study we report on the kinetic, crystallographic, modeling, and in vivo experiments of five pyrimidinyl phosphonucleotides with BS-RNase. These compounds are potent inhibitors of BS-RNase and can be the starting point for the rational design of new inhibitors with improved potency. Each inhibitor binds at the catalytic site by anchoring the pyrimidine at the B_1 subsite packed against the phenyl ring of Phe120 and its 2′-hydroxyl group is in hydrogen bonding distance from the side chain atoms of Thr45, while the rest of the ligand adopts a different conformation for each inhibitor (Figs. 3 and 4). This binding mode shows the strong specificity of subsite B_1 for pyrimidinyl compounds. The phosphate groups bind according to their position in the ligand molecule, i.e. 3′ phosphates binds at P_1 and 5′ phosphates binds at P_0 following the pattern that substrate RNA might bind. In addition, the 2′phosphate binds also at P_1. Subsite P_1 shows a clear preference for 3′ phosphate groups over 5′ since in the binding of U3′p, and C3′p the 3′-phosphate group is bound at P_1 while in the case of UDP and C5′p the 5′-phosphate group is bound away from P_1 to P_0 (Fig. 4). However, it is not clear whether a 2′- over a 5′-phosphate group is preferable at P_1, as the enzyme could bind both phosphate groups equally well. It seems that the answer may lie in the conformation of the bound nucleotide which is always *anti*, the preferred conformation for the bound nucleotides [50]. This is also supported by previous observations in RNase A complexes where the binding of either the 3′- or the 5′-phosphate group at P_1 was accompanied by a change from the *anti* to the *syn* conformation of an adenosine [54,71,72]. The binding of either the 2′- or the 3′-phosphate group to P_1 does not seem to affect significantly the binding mode of uridine to subsite B_1 since the phosphate group, in each case, finds favorable interactions with the enzyme (Fig. 4A). This has been also

observed in RNase A complexes with various uridylyl nucleotides [54,72,73].

The BS-RNase complex structures, described in this work, suggest how further development of tight binding inhibitors of RNases could be achieved through structure driven design. The binding of the 3′ and 5′ phosphates at different subsites implies that a 3′,5′ diphosphonucleotide might have a better potency than the monophosphate ones since it will allow the exploitation of the interactions with the protein at both subsites. The high resolution of the crystal structures in the present study, allowed also the identification of a large number of water molecules in the active site with bound inhibitors. Several of these water molecules mediate interactions between the inhibitors and the protein and their positions could be the starting point for the design of more potent inhibitors. The uracyl in all complexes is involved in water mediated interactions with Ser123 and the side chain of Asp83 (Table 4). These water positions are conserved in all five complexes indicating positions with high potential to form hydrogen bonds with the protein. Introduction of various substituents to decorate these ligands with groups that will allow them to reach those water positions and exploit interactions with the protein could lead to an increase of the potency. However, the presence of the phosphate groups in the chemical structure of the studied inhibitors impedes any potential pharmaceutical use since (i) the biological half-live of phosphate compounds in vivo is limited [74], (ii) the high charge of phosphate groups impedes these molecules from achieving high concentrations at the target site due to low oral bioavailability and/or cell penetration [61] (iii) such compounds occur naturally and bind to a broad range of proteins [75] and (iv) their instability in vivo due to the presence of a variety of phosphodiesterases and hydrolases [61]. An alternative solution to the above obstacles might be the replacement of the phosphate groups by methylene phosphonates or fluorophosphonates [75] or to use a prodrug strategy such as the use of phosphonic diamides instead of phosphonates [61].

Although a crystal structure of the human pancreatic ribonuclease (HP-RNase) has not been reported yet and the solution structure of native HP-RNase has recently been reported [76], there are crystal structures for few HP-RNase variants A [22,28,77–79]. These variants were produced by transferring some of the structural characteristics of BS-RNase responsible for its antitumor properties to HP-RNase with the goal to produce a chemotherapeutic agent tolerated by the immune system. Structural comparison of these mutant structures of HP-RNase with the structure of each of the five BS-RNase inhibitor complexes revealed that all five of the ligands could be accommodated within the active site of the HP-RNase variant without any difficulties. This was anticipated since the active site of HP-RNase is conserved in BS-RNase. This finding supports the hypothesis that inhibitors can have a role as modulators of a potential chemotherapeutic agent based on a variant of HP-RNase with the antitumor properties of BS-RNase. However, it also emphasizes the need to introduce modifications to the inhibitors that will enhance their specificity towards such a variant. On the other hand it may be possible to introduce some modifications to the active site of the HP-RNase variant to enhance its preference for a given inhibitor.

Nevertheless, the studied compounds can only serve as potential scaffolds for further development. Hence, calculation of their pharmacokinetic properties and in-vivo activity at an early stage such as this can help to optimize the design of future inhibitors/scaffolds in a step-wise manner, with the aim not only to improve inhibitory potential but also the equally important pharmacokinetic and in-vivo properties. ADME property predictions using QikProp revealed ligands U2′p and U3′p to have oral drug-like properties based on Lipinski's rule of 5. These two inhibitors together with C5′p have only one property outside the range observed for 95% of drugs. Previously, we have shown through molecular dynamics studies that polar phosphate groups increase inhibitory potential of nucleotide based inhibitors mainly through electrostatic interactions [80]. However, based on the ADME criteria of Veber and co-workers and the range in properties for 95% of known drugs, the number or H-bond acceptors/polar surface area properties needs to be reduced for oral bioavailability of future analogues developed based on phosphonucleotide derivatives. In future work, we will also evaluate potential effects of the applied dose of nucleotides in vivo experiments and consider any additional toxic side effect that the nucleotides might present, considering that nucleotide analogues can be carcinogenic and may also interact with other nucleases or nucleotide binding proteins.

We also showed that the cytidine inhibitors have a significant effect in the aspermatogenic effect of BS-RNase in mice (Fig. 7) confirming our hypothesis that BS-RNase inhibitors may have a potential as antidotes to the severe side-effects that accompany the BS-RNase anticancer activity. This finding emphasizes even further the importance of the continuation of our rational design efforts towards the development of stable, selective, and potent inhibitors for BS-RNase.

A high throughput screening of small-molecule chemical libraries like those used for human angiogenin [81–83] as well as a proteomic approach to screen and analyze nucleotide binding proteins could be interesting for future considerations of nucleotide analogues in the search for potential efficient low-molecular-weight inhibitors RNase inhibitors and we are currently pursuing these directions.

4. Experimental protocols

4.1. Kinetic experiments

BS-RNase was purified as described previously [15]. Nucleotide inhibitors and C > p were obtained from Sigma (Greece). Concentrations of RNase A, BS-RNase and C > p samples were determined spectrophotometrically ($\epsilon_{278} = 9800\ M^{-1}\,cm^{-1}$ [15,84]; $\epsilon_{268} = 8400\ M^{-1}\,cm^{-1}$ [85]). Enzymatic activity of BS-RNase and RNase A was measured by a spectrophotometric method [86]. All assays were performed in duplicates at 30 °C in 0.1 M MES/NaOH buffer (pH 6.0) containing 0.1 M NaCl with enzyme concentration of 1.0 μM. The activity was measured by following the initial reaction velocities, using the difference molar absorbance coefficient $\Delta\epsilon_{278} = 516.4\ M^{-1}\,cm^{-1}$ for the hydrolysis reaction of C > p [87]. The inhibition constants (K_i) were determined by the Dixon method [88] using non-linear regression analysis with the program GRAFIT [89] (Table 1).

4.2. Crystallization, data collection and structure refinement

BS-RNase crystals were grown using the vapour diffusion method with protein concentration of 10 mg/ml in 15% w/v PEG 4000, 50 mM sodium acetate, and 50 mM Tris/HCl buffer pH 8.5 equilibrated against a reservoir solution containing in 30% w/v PEG 4000, 0.1 M sodium acetate, and 0.1 M Tris/HCl buffer pH 8.5 at 16 °C [90]. The crystals belong to space group $P2_12_12_1$ with one homodimer per asymmetric unit and cell dimensions $a = 48.6$ Å, $b = 59.0$ Å and $c = 82.2$ Å. Crystals of the inhibitor complexes were obtained by soaking single BS-RNase crystals with a buffered solution (30% w/v PEG 4000, 0.1 M sodium acetate, and 0.1 M Tris/HCl pH 8.5) of each of the inhibitor prior to data collection (Table 2).

Diffraction data for the complexes were collected at 100 K at the EMBL stations X11 ($\lambda = 0.8148$ Å) and X13 ($\lambda = 0.8088$ Å) at the DORIS storage ring, DESY, Hamburg, using a MARCCD detector. Raw data were processed with the HKL suite of programs [91] and intensities were transformed to amplitudes with TRUNCATE [92].

Phases were obtained using the structure of the free BS-RNase [pdb code: 1r5d; [36]] as a starting model. Alternate cycles of manual building with the program COOT [93], and refinement using the maximum likelihood target function as implemented in the program REFMAC [94], improved the model, while inhibitor molecules were included during the final stages of the refinement. A final round of TLS (Translation/Libration/Screw) refinement within the program REFMAC [94] using TLS groups for the protein, generated by the TLSMD web server [95] improved considerably the final model. Details of data processing and refinement statistics are provided in Table 2. The program PROCHECK [96] was used to assess the quality of the final structure. Analysis of the Ramachandran (ϕ–ψ) plot showed that all residues lie in the allowed regions. Solvent accessible areas were calculated with the program NACCESS [97]. The atomic coordinates and the X-ray amplitudes for the BS-RNase – inhibitor complexes have been deposited in the Research Collaboratory for Structural Bioinformatics Protein Data Bank, (http://www.rcsb.org) (accession IDs are shown in Table 2). Figures prepared with the programs MOLSCRIPT [98] or BOBSCRIPT [99] and rendered with Raster3D [100].

4.3. Spermatogenic toxicity in mice

The effect of the most potent inhibitors C3′p and C5′p on the aspermatogenic action of BS-RNase was determined on adult male ICR mice [17,60,101]. The spermatogenic assays have been performed according to the method established previously [60], and sexually adult male mice were injected with 10 μg of BS-RNase (a typical dose) or with a mixture of 10 μg BS-RNase with the inhibitor (w/w ratios of 1:1 or 1:100) once into left testes. Ten days after the injection, the animals were sacrificed, their testicles excised and studied by histology examination. Body weight of the treated mice was determined in the course of the experiment. Degenerative effects on the testes were assessed such as decreased weight of the testes, decreased width of the spermatogenic layers and reduced seminiferous tubules diameter.

4.4. Modeling

ADME properties of the analogues were predicted using the QikProp program (QikProp, version 3.1) in normal mode. All the analogues were prepared in neutralized form for use with QikProp using Schrodinger's Maestro Build module and LigPrep. The input conformation for the QikProp calculations was determined as follows: 500 steps of a Monte Carlo Multiple Minima (MCMM) search [102] for each molecule in H_2O, modeled using the GB/SA continuum model [103], was first performed. The OPLS-AA (2005) force field was used [104,105]. An energy window for saving unique conformations of 21.0 kJ/mol (~5 kcal/mol) was used. QikProp shows slight dependence on input conformation with a more extended conformation yielding better results. Therefore, output conformations from the Monte Carlo (MC) search were clustered into five groups with the lowest energy conformer from the most extended conformation family chosen. Clustering was performed using the XCluster program (MacroModel XCluster, version 9.6) using heavy atoms for atom superimposition and comparisons, with redundant/duplicate conformers eliminated based on a cut-off RMSD criterion of 0.5 Å.

Acknowledgments

This work was supported by the Hellenic General Secretariat for Research and Technology (GSRT), and the Minister of Education, Youth and Sports of the Czech Republic through a Joint Research and Technology project between Greece and The Czech Republic (2006–2008) (to D.D.L. and P.P.). J.M. is obliged to the Grant Agency of the Czech Republic for the grants No.523/06/1149 and No. 521/06/1149 and to the League against Cancer, Prague, Czech Republic for support. D.D.L. also acknowledges the support of the Commission of the European Communities – under the FP7 "SP4-Capacities Coordination and Support Action, Support Actions" EUROSTRUCT project (CSA-SA_FP7-REGPOT-2008-1 Grant Agreement N° 230146). This work was also supported by grants from European Community – Research Infrastructure Action under the FP6 "Structuring the European Research Area" Programme (through the Integrated Infrastructure Initiative "Integrating Activity on Synchrotron and Free Electron Laser Science") for work at the Synchrotron Radiation Source, CCLRC, Daresbury U.K., MAX-lab, Lund, Sweden, and EMBL Hamburg Outstation, Germany. We gratefully acknowledge MAX-lab (Lund, Sweden), EMBL Outstation at DESY (Hamburg, Germany), and SRS (Daresbury, U.K.) for provision of synchrotron-radiation facilities.

References

[1] J. Matousek, Comp. Biochem. Physiol. C Toxicol. Pharmacol. 129 (2001) 175–191.
[2] M.R. Mastronicola, R. Piccoli, G. D'Alessio, Eur. J. Biochem. 230 (1995) 242–249.
[3] P. Laccetti, G. Portella, M.R. Mastronicola, A. Russo, R. Piccoli, G. D'Alessio, G. Vecchio, Cancer Res. 52 (1992) 4582–4586.
[4] P. Laccetti, D. Spalletti-Cernia, G. Portella, P. De Corato, G. D'Alessio, G. Vecchio, Cancer Res. 54 (1994) 4253–4256.
[5] J. Soucek, P. Pouckova, J. Matousek, P. Stockbauer, J. Dostal, M. Zadinova, Neoplasma 43 (1996) 335–340.
[6] P. Pouckova, J. Soucek, J. Jelinek, M. Zadinova, D. Hlouskova, J. Polivkova, L. Navratil, J. Cinatl, J. Matousek, Neoplasma 45 (1998) 30–34.
[7] J. Cinatl Jr., J. Cinatl, R. Kotchetkov, J.U. Vogel, B.G. Woodcock, J. Matousek, P. Pouckova, B. Kornhuber, Int. J. Oncol. 15 (1999) 1001–1009.
[8] L. Vitagliano, S. Adinolfi, F. Sica, A. Merlino, A. Zagari, L. Mazzarella, J. Mol. Biol. 293 (1999) 569–577.
[9] V. Cafaro, C. De Lorenzo, R. Piccoli, A. Bracale, M.R. Mastronicola, A. Di Donato, G. D'Alessio, FEBS Lett. 359 (1995) 31–34.
[10] J.S. Kim, J. Soucek, J. Matousek, R.T. Raines, J. Biol. Chem. 270 (1995) 10525–10530.
[11] J.S. Kim, J. Soucek, J. Matousek, R.T. Raines, Biochem. J. 308 (1995) 547–550.
[12] A. Antignani, M. Naddeo, M.V. Cubellis, A. Russo, G. D'Alessio, Biochemistry 40 (2001) 3492–3496.
[13] J. Matousek, P. Pouckova, J. Soucek, J. Skvor, J. Control. Release 82 (2002) 29–37.
[14] M. Michaelis, J. Cinatl, P. Pouckova, K. Langer, J. Kreuter, J. Matousek, Anticancer Drugs 13 (2002) 149–154.
[15] J. Dostal, J. Matousek, J. Reprod. Fertil. 33 (1973) 263–274.
[16] J. Matousek, J. Reprod. Fertil. 32 (1973) 175–184.
[17] J. Matousek, J. Reprod. Fertil. 43 (1975) 171–174.
[18] T. Slavik, J. Matousek, J. Fulka, R.T. Raines, J. Exp. Zool. 287 (2000) 394–399.
[19] J. Soucek, V. Chudomel, I. Potmesilova, J.T. Novak, Nat. Immun. Cell Growth Regul. 5 (1986) 250–258.
[20] M. Tamburrini, G. Scala, C. Verde, M.R. Ruocco, A. Parente, S. Venuta, G. D'Alessio, Eur. J. Biochem. 190 (1990) 145–148.
[21] P.A. Leland, R.T. Raines, Chem. Biol. 8 (2001) 405–413.
[22] A. Merlino, G. Avella, S. Di Gaetano, A. Arciello, R. Piccoli, L. Mazzarella, F. Sica, Protein Sci. 18 (2009) 50–57.
[23] P.A. Leland, K.E. Staniszewski, B.M. Kim, R.T. Raines, J. Biol. Chem. 276 (2001) 43095–43102.
[24] A. Merlino, C. Ercole, D. Picone, E. Pizzo, L. Mazzarella, F. Sica, J. Mol. Biol. 376 (2008) 427–437.
[25] A. Merlino, I.R. Krauss, M. Perillo, C.A. Mattia, C. Ercole, D. Picone, A. Vergara, F. Sica, Biopolymers (2009).
[26] C. Ercole, R.A. Colamarino, E. Pizzo, F. Fogolari, R. Spadaccini, D. Picone, Biopolymers (2009).
[27] M. Libonati, Comp. Biochem. Physiol. Biochem. Mol. Biol. 61 (2004) 2431–2446.
[28] A. Canals, J. Pous, A. Guasch, A. Benito, M. Ribo, M. Vilanova, M. Coll, Structure 9 (2001) 967–976.
[29] Y. Liu, G. Gotte, M. Libonati, D. Eisenberg, Nat. Struct. Biol. 8 (2001) 211–214.
[30] J.E. Lee, R.T. Raines, Biochemistry 44 (2005) 15760–15767.
[31] I. Bjork, U. Lindahl, Mol. Cell. Biochem. 48 (1982) 161–182.
[32] Y.J. Chuang, R. Swanson, S.M. Raja, S.T. Olson, J. Biol. Chem. 276 (2001) 14961–14971.
[33] A. Joost, V. Kurowski, P.W. Radke, Curr. Pharm. Des. 14 (2008) 1176–1185.
[34] M. Famulok, Nat. Biotechnol. 22 (2004) 1373–1374.
[35] L. Mazzarella, S. Capasso, D. Demasi, G. Di'Lorenzo, C.A. Mattia, A. Zagari, Acta Crystallogr. D49 (1993) 389–402.

[36] A. Merlino, L. Vitagliano, F. Sica, A. Zagari, L. Mazzarella, Biopolymers 73 (2004) 689–695.
[37] L. Vitagliano, S. Adinolfi, A. Riccio, F. Sica, A. Zagari, L. Mazzarella, Protein Sci. 7 (1998) 1691–1699.
[38] A. Floridi, G. D'Alessio, E. Leone, Eur. J. Biochem. 26 (1972) 162–167.
[39] C.A. Lipinski, F. Lombardo, B.W. Dominy, P.J. Feeney, Adv. Drug Deliv. Rev. 23 (1997) 3–25.
[40] C.A. Lipinski, J. Pharmacol. Toxicol. Methods 44 (2000) 235–249.
[41] D.F. Veber, S.R. Johnson, H.Y. Cheng, B.R. Smith, K.W. Ward, K.D. Kopple, J. Med. Chem. 45 (2002) 2615–2623.
[42] D.G. Anderson, G.G. Hammes, F.G. Walz, Biochemistry 7 (1968) 1637–1645.
[43] D.D. Leonidas, T.K. Maiti, A. Samanta, S. Dasgupta, T. Pathak, S.E. Zographos, N.G. Oikonomakos, Bioorg. Med. Chem. 14 (2006) 6055–6064.
[44] N. Borkakoti, D.A. Moss, R.A. Palmer, Acta Crystallogr. B38 (1982) 2210–2217.
[45] B. Howlin, D.S. Moss, G.W. Harris, Acta Crystallogr. A45 (1989) 851–861.
[46] V.S.J. deMel, M.S. Doscher, P.D. Martin, B.F.P. Edwards, FEBS Lett. 349 (1994) 155–160.
[47] L. Mazzarella, S. Capasso, D. Demasi, G. Di Lorenzo, C.A. Mattia, A. Zagari, Acta Crystallogr. D Biol. Crystallogr. 49 (1993) 389–402.
[48] R. Berisio, V.S. Lamzin, F. Sica, K.S. Wilson, A. Zagari, L. Mazzarella, J. Mol. Biol. 292 (1999) 845–854.
[49] A.A. Fedorov, D. Joseph-McCarthy, E. Fedorov, D. Sirakova, I. Graf, S.C. Almo, Biochemistry 35 (1996) 15962–15979.
[50] S.L. Moodie, J.M. Thornton, Nucleic Acids. Res. 21 (1993) 1369–1380.
[51] J.C. Fontecilla-Camps, R. de Llorens, M.H. le Du, C.M. Cuchillo, J. Biol. Chem. 269 (1994) 21526–21531.
[52] B.M. Fisher, J.E. Grilley, R.T. Raines, J. Biol. Chem. 273 (1998) 34134–34138.
[53] G.N. Hatzopoulos, D.D. Leonidas, R. Kardakaris, J. Kobe, N.G. Oikonomakos, FEBS J. 272 (2005) 3988–4001.
[54] D.D. Leonidas, G.B. Chavali, N.G. Oikonomakos, E.D. Chrysina, M.N. Kosmopoulou, M. Vlassi, C. Frankling, K.R. Acharya, Protein Sci. 12 (2003) 2559–2574.
[55] I. Zegers, D. Maes, M.H. Dao-Thi, F. Poortmans, R. Palmer, L. Wyns, Protein Sci. 31 (1994) 2322–2339.
[56] C.F. Aguilar, P.J. Thomas, A. Mills, D.S. Moss, R.A. Palmer, J. Mol. Biol. 224 (1992) 265–267.
[57] H. Witzel, E.A. Barnard, Biochem. Biophys. Res. Commun. 7 (1962) 295–299.
[58] A. Russo, K.R. Acharya, R. Shapiro, Methods Enzymol. 341 (2001) 629–648.
[59] D.D. Leonidas, R. Shapiro, S.C. Allen, G.V. Subbarao, K. Veluraja, K.R. Acharya, J. Mol. Biol. 285 (1999) 1209–1233.
[60] J. Matousek, J.S. Kim, J. Soucek, J. Riha, M. Ribo, P.A. Leland, R.T. Raines, Comp. Biochem. Physiol. Biochem. Mol. Biol. 118 (1997) 881–888.
[61] S.J. Hecker, M.D. Erion, J. Med. Chem. 51 (2008) 2328–2345.
[62] A. Ogawa, M. Tanaka, T. Sasaki, A. Matsuda, J. Med. Chem. 41 (1998) 5094–5107.
[63] M.P. Sandrini, A.R. Clausen, S.L. On, F.M. Aarestrup, B. Munch-Petersen, J. Piskur, J. Antimicrob. Chemother. 60 (2007) 510–520.
[64] C.M. Galmarini, J.R. Mackey, C. Dumontet, Lancet Oncol. 3 (2002) 415–424.
[65] P. Artursson, J. Karlsson, Biochem. Biophys. Res. Commun. 175 (1991) 880–885.
[66] P. Artursson, K. Palm, K. Luthman, Adv. Drug. Deliv. Rev. 46 (2001) 27–43.
[67] K. Palm, K. Luthman, A.L. Ungell, G. Strandlund, P. Artursson, J. Pharm. Sci. 85 (1996) 32–39.
[68] K. Palm, P. Stenberg, K. Luthman, P. Artursson, Pharm. Res. 14 (1997) 568–571.
[69] J.J. Lu, K. Crimin, J.T. Goodwin, P. Crivori, C. Orrenius, L. Xing, P.J. Tandler, T.J. Vidmar, B.M. Amore, A.G.E. Wilson, P.F.W. Stouten, P.S. Burton, J. Med. Chem. 47 (2004) 6104–6107.
[70] W.L. Jorgensen, E.M. Duffy, Adv. Drug. Deliv. Rev. 54 (2002) 355–366.
[71] D.D. Leonidas, R. Shapiro, L.I. Irons, N. Russo, K.R. Acharya, Biochemistry 36 (1997) 5578–5588.
[72] A.M. Jardine, D.D. Leonidas, J.L. Jenkins, C. Park, R.T. Raines, K.R. Acharya, R. Shapiro, Biochemistry 40 (2001) 10262–10272.
[73] D.D. Leonidas, R. Shapiro, L.I. Irons, N. Russo, K.R. Acharya, Biochemistry 38 (1999) 10287–10297.
[74] A. Guranowski, Pharmacol. Ther. 87 (2003) 117–139.
[75] A. Guranowski, Acta Biochim. Pol. 50 (2003) 947–972.
[76] K.E. Kover, M. Bruix, J. Santoro, G. Batta, D.V. Laurents, M. Rico, J. Mol. Biol. 379 (2008) 953–965.
[77] J. Pous, A. Canals, S.S. Terzyan, A. Guasch, A. Benito, M. Ribo, M. Vilanova, M. Coll, J. Mol. Biol. 303 (2000) 49–59.
[78] J. Pous, G. Mallorqui-Fernandez, R. Peracaula, S.S. Terzyan, J. Futami, H. Tada, H. Yamada, M. Seno, R. de Llorens, F.X. Gomis-Ruth, M. Coll, Acta. Crystallogr. D. Biol. Crystallogr. 57 (2001) 498–505.
[79] H. Yamada, T. Tamada, M. Kosaka, K. Miyata, S. Fujiki, M. Tano, M. Moriya, M. Yamanishi, E. Honjo, H. Tada, T. Ino, H. Yamaguchi, J. Futami, M. Seno, T. Nomoto, T. Hirata, M. Yoshimura, R. Kuroki, Protein Sci. 16 (2007) 1389–1397.
[80] S. Polydoridis, D.D. Leonidas, N.G. Oikonomakos, G. Archontis, Biophys. J. 92 (2007) 1659–1672.
[81] J.L. Jenkins, R.Y. Kao, R. Shapiro, Proteins 50 (2003) 81–93.
[82] J.L. Jenkins, R. Shapiro, Biochemistry 43 (2003) 6674–6687.
[83] R.Y. Kao, J.L. Jenkins, K.A. Olson, M.E. Key, J.W. Fett, R. Shapiro, Proc. Natl. Acad. Sci. U.S.A. 99 (2002) 10066–10071.
[84] M. Sela, C.B. Anfinsen, Biochim. Biophys. Acta 24 (1957) 229–235.
[85] E. Boix, Z. Nikolovski, G.P. Moiseyev, H.F. Rosenberg, C.M. Cuchillo, M.V. Nogu ıs, J. Biol. Chem. 274 (1999) 15605–15614.
[86] A. Samanta, D.D. Leonidas, S. Dasgupta, T. Pathak, S.E. Zographos, N.G. Oikonomakos, J. Med. Chem. 52 (2009) 932–942.
[87] E. Boix, M.V. Nogues, C.H. Schein, S.A. Benner, C.M. Cuchillo, J. Biol. Chem. 269 (1994) 2529–2534.
[88] M. Dixon, Biochem. J. 55 (1953) 170–171.
[89] Leatherbarrow RJ. Erithacus Software Ltd Staines, U.K.; 1992.
[90] F. Sica, S. Adinolfi, R. Berisio, C. De Lorenzo, L. Mazzarella, R. Piccoli, L. Vitagliano, A. Zagari, J. Cryst. Growth 196 (1999) 305–312.
[91] Z. Otwinowski, W. Minor, Processing of X-ray diffraction data collected in oscillation mode, in: C.W.J. Carter, R.M. Sweet (Eds.), Methods in Enzymology, vol. 276, Academic Press, New York, 1997, pp. 307–326.
[92] S. French, K.S. Wilson, Acta. Crystallogr. A34 (1978) 517–525.
[93] P. Emsley, K. Cowtan, Acta. Crystallogr. D. Biol. Crystallogr. 60 (2004) 2126–2132.
[94] G.N. Murshudov, A.A. Vagin, E.J. Dodson, Acta. Crystallogr. D53 (1997) 240–255.
[95] J. Painter, E.A. Merritt, J. Appl. Crystallogr. 39 (2005) 109–111.
[96] R.A. Laskowski, M.W. MacArthur, D.S. Moss, J.M. Thornton, J. Appl. Crystallogr. 26 (1993) 283–291.
[97] Hubbard SJ, Thornton JM. 1993.
[98] P.J. Kraulis, J. Appl. Crystallogr. 24 (1991) 946–950.
[99] R.M. Esnouf, J. Mol. Graph. Model. 15 (1997) 132–134.
[100] E.A. Merritt, D.J. Bacon, Method Enzymol B277 (1997) 505–524.
[101] J. Matousek, R. Stanek, J. Dostal, J. Macha, Folia Biol. (Praha) 25 (1979) 36–48.
[102] G. Chang, W.C. Guida, W.C. Still, J. Am. Chem. Soc. 111 (1989) 4379–4386.
[103] W.C. Still, A. Tempczyk, R.C. Hawley, T. Hendrickson, J. Am. Chem. Soc. 112 (1990) 6127–6129.
[104] W.L. Jorgensen, D.S. Maxwell, J. Tirado-Rives, J. Am. Chem. Soc. 118 (1996) 11225–11236.
[105] G.A. Kaminski, R.A. Friesner, J. Tirado-Rives, W.L. Jorgensen, J. Phys. Chem. B 105 (2001) 6474–6487.
[106] A.T. Brünger, Nature 355 (1992) 472–475.
[107] Iupac-Iub, J. C. o. B.N. (JCBN), Eur. J. Biochem. 131 (1983) 5–7.
[108] C. Altona, M. Sundaralingam, J. Am. Chem. Soc. 94 (1972) 8205–8212.
[109] I.K. McDonald, J.M. Thornton, J. Mol. Biol. 238 (1994) 777–793.